Available online at www.sciencedirect.com

ScienceDirect

Procedia Engineering 163 (2016) 315 – 327

Procedia Engineering

www.elsevier.com/locate/procedia

25th International Meshing Roundtable (IMR25)

Generation of curved high-order meshes with optimal quality and geometric accuracy

Eloi Ruiz-Gironés[a,*], Josep Sarrate[a], Xevi Roca[b]

[a]*Laboratori de Càlcul Numèric (LaCàN), Departament d'Enginyeria Civil i Ambiental, Universitat Politècnica de Catalunya (UPC), Campus Nord UPC, 08034 Barcelona, Spain.*

[b]*Computer Applications in Science and Engineering, Barcelona Supercomputing Center, 08034 Barcelona, Spain*

Abstract

We present a novel methodology to generate curved high-order meshes featuring optimal mesh quality and geometric accuracy. The proposed technique combines a distortion measure and a geometric $\mathcal{L}_2$-disparity measure into a single objective function. While the element distortion term takes into account the mesh quality, the $\mathcal{L}_2$-disparity term takes into account the geometric error introduced by the mesh approximation to the target geometry. The proposed technique has several advantages. First, we are not restricted to interpolative meshes and therefore, the resulting mesh approximates the target domain in a non-interpolative way, further increasing the geometric accuracy. Second, we are able to generate a series of meshes that converge to the actual geometry with expected rate while obtaining high-quality elements. Third, we show that the proposed technique is robust enough to handle real-case geometries that contain gaps between adjacent entities.

Peer-review under responsibility of the organizing committee of IMR 25

Keywords: Curved high-order mesh, non-interpolative mesh, disparity measure, geometric accuracy, distortion measure

1. Introduction

Unstructured high-order methods [1–5] have been shown to be well suited to tackle problems where geometrical flexibility, high accuracy, and low numerical dissipation and dispersion are needed. Remarkably, high-order methods feature exponential converge rates and therefore, they have been proved to be faster than low-order methods in several applications [6–14], especially in those problems where an implicit solver is required [15]. Moreover, high-order unstructured methods can use curved meshes to approximate the geometry, thus reducing the spurious numerical artifacts that may arise from a piecewise linear approximation of the curved domain boundaries [16–22].

Unstructured high-order methods rely on a curved high-order mesh that approximates the physical domain. To enable the benefits of these methods, curved high-order meshes have two requirements. First, the mesh has to be valid, in the sense that there are not any inverted elements. Even more, the curved mesh has to be composed of high-quality elements since only one low-quality element can lead to ill-conditioned linear systems [23]. In that case,

* Corresponding author.
E-mail address: eloi.ruiz@upc.edu

Peer-review under responsibility of the organizing committee of IMR 25
doi:10.1016/j.proeng.2016.11.108

the approximation accuracy is degraded and the solution may be polluted by the introduced error. A curved mesh is considered to be of high-quality if all the elements have a shape close to regular (smooth and well-conditioned Jacobian). Second, the geometric error introduced by the approximation of the target domain by curved elements has to be bounded. Otherwise, the geometric error may pollute the numerical solution and the convergence rate of unstructured high-order methods can be lost.

One of the most common methods to generate a curved high-order mesh is the *a posteriori* approach [6,18,24–39]. In this approach, an initial mesh, composed of elements of the required shape and size, is curved to properly approximate the boundaries of the target domain while maintaining valid and high-quality elements.

The main contribution of this work is the generation of optimal curved high-order meshes in the sense of element quality and geometric accuracy. To this end, we describe a novel *a posteriori* methodology that relies on two different techniques. On the one hand, similarly to the work presented in [22], we use a point-wise distortion measure to determine the validity of the mesh. Moreover, we use a regularized [40–44] point-wise distortion measure to formulate a global optimization problem that allows curving the high-order mesh in order to obtain a valid mesh composed of high-quality elements. On the other hand, we use an $\mathcal{L}_2$-disparity measure [45] to quantify the deviation between a curved high-order mesh and a parameterized m-dimensional manifold embedded in an n-dimensional space. Thus, we are able to measure a *distance* between a mesh and a manifold and therefore, we can improve the geometric approximation of the target domain. Combining these techniques, we formulate a global problem that takes into account both the element quality and the geometric error. In our setup, we do not impose that the boundary nodes have to be on their corresponding geometric entities. Thus, the resulting mesh is not interpolative anymore although the geometric approximation of the optimized mesh is improved with respect to the geometric approximation of the initial one, in the sense of the $\mathcal{L}_2$-disparity measure.

The proposed methodology has several advantages. First, we show that the high-order mesh optimally converges to the actual geometry in the $\mathcal{L}_2$-disparity sense. Thus, the geometric error is bounded and therefore, unstructured high-order methods can obtain numerical solutions that optimally convergence to the actual solution. Second, we show that the proposed technique can be applied to real-case geometries that contain gaps between adjacent entities. Note that this is common in complex geometries because the involved procedures introduce numerical errors. As long as the errors are below e prescribed tolerance, the CAD model is considered valid.

The rest of the paper is organized as follows. In Section 2, we review previous literature relevant to this work. In Section 3.1 we present a simple example to motivate this work. In Section 3.2, we introduce several definitions related to this work. Section 3.3 deals with the distortion measure and how to curve a high-order mesh. Section 3.4 presents the $\mathcal{L}_2$-disparity measure. Section 4 presents the coupled optimization of the distortion and $\mathcal{L}_2$-disparity measures. Finally, in Section 5, we present several examples to illustrate the application of the proposed method.

2. Related Work

In this work, we adopt an *a posteriori* approach [6,18,24–39] to generate curved high-order meshes. Given a linear mesh, the polynomial degree of the elements is increased and the mesh is curved to match the geometry. We highlight that the main challenge of *a posteriori* mesh deformation methods is to repair the invalid elements that may arise when approximating the boundary of the domain.

While most of the methods fix the position of boundary nodes, other approaches allow to move them. Note that the main issue is to impose that the boundary nodes should approximate the geometry boundary. To this end, it is possible to include a penalty term in the objective function that enforces that the corresponding nodes move close to the boundary [46]. It is also possible to impose that the nodes are strictly on the boundary of the geometry. In [47] the authors proposed a mesh quality improvement method that relocates the volume and surface nodes, but not the curve nodes. In some applications, such as curved high-order mesh generation with structured meshing, it could be also required to move the curve nodes. It is possible to express the proposed objective function in terms of the parametric coordinates of the boundary nodes and the physical coordinates of the inner nodes. For instance, in [35] the authors minimize an objective function that penalizes both large deformations and small values of the determinant of the iso-parametric mapping, and in [39], the authors minimize an objective function that penalizes high distortions of the mesh.

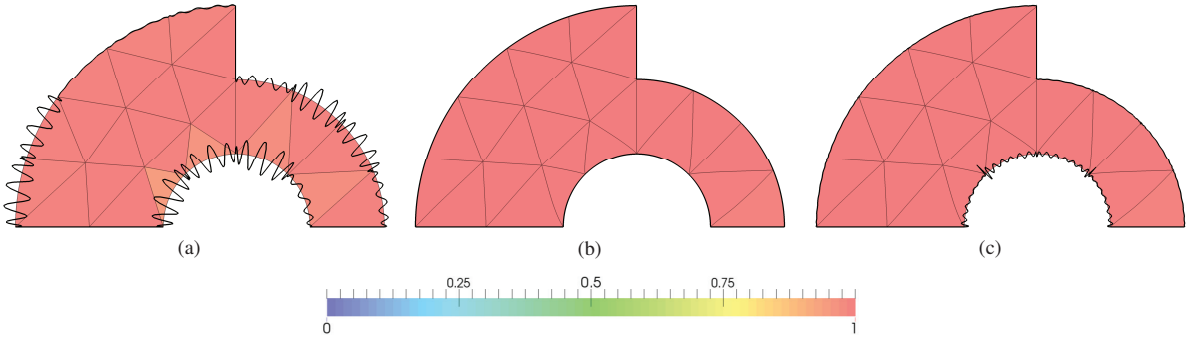

Fig. 1. Triangular meshes of polynomial degree ten, elements colored by quality, and geometric error at the boundary (thick line): (a) original interpolative mesh, geometric error amplified by a factor of 10^5; (b) optimized non-interpolative mesh, geometric error amplified by a factor of 10^5; and (c) optimized non-interpolative mesh, geometric error amplified by a factor of 10^9.

However, none of the previous techniques take into account the geometric errors when approximating the boundary of the geometry, since they assume that it is enough to locate the nodes on the geometric entities to correctly approximate the domain. In [48], the authors introduce an area-based distance to measure the distance between a curved high-order mesh and a curve in the 2D plane. Then, they optimize the area-based distance at the same time as the minimum Jacobian of the iso-parametric mapping. In [49], the authors introduce a Taylor-based distance for planar meshes and curves. Basically, the Taylor distance consists on checking the difference between the tangent and curvature vectors at the interpolation points of the curve. For the three-dimensional case, the Taylor distance is defined as the difference of the normal vectors of the mesh and the surface at the interpolation points. In reference [45], we introduced an $\mathcal{L}_2$-disparity measure between a curved high-order mesh and a manifold. Thus, we are able to check the geometric accuracy of a curved high-order mesh. In addition, we proposed to optimize an objective function related to the $\mathcal{L}_2$-disparity to improve the accuracy of the high-order mesh.

In this work, we optimize a curved high-order mesh by taking into account the distortion of the mesh as well as the $\mathcal{L}_2$-disparity between the mesh and the target geometry. The main difference between the proposed approach and previous attempts to combine an untangling objective function and a geometric accuracy measure is that we are not imposing an interpolative mesh. Thus, we are able to further increase the geometric accuracy and obtain the expected convergence rate of the mesh to the actual geometry.

3. Preliminaries

3.1. Motivation

To illustrate that our methodology is able to optimize a mesh by taking into account both the element quality and the geometric approximation error, we consider a simple toy geometry. Figure 1(a) shows an initial triangular mesh composed of curved high-order elements of degree ten, where we have colored the elements according to the shape quality measure. The black line corresponds to the geometric error of the mesh amplified by a factor of 10^5. Note that this mesh is interpolative and therefore, the geometric error is exactly zero at the interpolation points. By moving the nodes of the mesh, we can obtain an optimized mesh in which the element quality is improved, and the geometric error is reduced, see Figure 1(b). In this figure, the geometric error is also amplified by a factor of 10^5. In order to visually notice the geometric error we have to amplify it by a factor of 10^9, see Figure 1(c). Note that in our approach, the boundary nodes are not imposed to be on the geometry in order to obtain an interpolative mesh. Thus, we generate a non-interpolative mesh that better approximates the target geometry than the initial mesh.

3.2. Definitions

We consider that a curved high-order mesh in the physical domain, $\mathcal{M}^P$, is composed of a set of elements, e^P, and that each element has a corresponding master element, e^M. Thus, the physical mesh can be defined in terms of an element-wise parameterization $\boldsymbol{\phi}^P$ in such a way that:

$$\begin{aligned} \boldsymbol{\phi}^P|_{\mathrm{e}^M} : \mathrm{e}^M &\longrightarrow \mathrm{e}^P \subset \mathbb{R}^n \\ \boldsymbol{\xi} &\longmapsto \mathbf{x} = \sum_{i=1}^{n_p} \mathbf{x}_i N_i^{\mathbf{x}}(\boldsymbol{\xi}), \end{aligned}$$

where $\boldsymbol{\xi}$ are the coordinates in the master element, n_p is the number of nodes of the high-order element e^P, $\mathbf{x}_i$ are the coordinates of the i-th node in the physical space, and $\{N_i^{\mathbf{x}}\}_{i=1,\dots,n_p}$ is a Lagrangian basis of polynomial shape functions of degree p defined in the master element. We define the master mesh, $\mathcal{M}^M$, as the mesh composed of all the master elements of the physical mesh, $\mathcal{M}^P$.

3.3. Quality and Distortion Measures

Let $\mathcal{M}^I$ be a straight-sided high-order mesh, composed of elements of the desired shape and size. In the *a posteriori* approach, we have to curve the elements of $\mathcal{M}^I$ in order to correctly approximate the geometry model. To this end, we deform the ideal mesh, $\mathcal{M}^I$, to obtain the physical mesh, $\mathcal{M}^P$, by means of a diffeomorphism $\boldsymbol{\phi}$. According to [22], we can obtain mapping $\boldsymbol{\phi}$ by optimizing the functional

$$E_Q(\boldsymbol{\phi}) = \|M\boldsymbol{\phi} - 1\|^2, \tag{1}$$

where $\|\cdot\|$ is the $\mathcal{L}_2$ norm of functions, and M is a regularized point-wise shape distortion measure defined as [40–42]

$$M\boldsymbol{\phi}(\mathbf{y}) = \frac{|\mathbf{D}\boldsymbol{\phi}(\mathbf{y})|^2}{n\sigma_\delta(\mathbf{D}\boldsymbol{\phi}(\mathbf{y}))^{2/n}},$$

being $|\cdot|$ the Frobenius norm of matrices, σ the determinant of $\mathbf{D}\boldsymbol{\phi}$ and

$$\sigma_\delta = \frac{1}{2}\left(\sigma + \sqrt{\sigma^2 + 4\delta^2}\right).$$

The point-wise distortion measure equals to one when the matrix $\mathbf{D}\boldsymbol{\phi}(\mathbf{y})$ is a rotation combined with an isotropic scaling, and it tends to infinity when $\mathbf{D}\boldsymbol{\phi}(\mathbf{y})$ becomes non-invertible. Note that the optimal mapping $\boldsymbol{\phi}$ should have a point-wise distortion measure equal to one everywhere. Since this is not always possible, in Equation (1) we impose the optimality condition in a least-squares sense.

Note that the mapping $\boldsymbol{\phi}$ can be defined as $\boldsymbol{\phi} = \boldsymbol{\phi}^P \circ \left(\boldsymbol{\phi}^I\right)^{-1}$, being $\boldsymbol{\phi}^P$ and $\boldsymbol{\phi}^I$ the mappings that transform the master mesh, $\mathcal{M}^M$, to the physical and ideal mesh, $\mathcal{M}^P$ and $\mathcal{M}^I$, respectively. Since $\boldsymbol{\phi}^P$ is defined in terms of the position of the physical nodes and $\boldsymbol{\phi}^I$ is fixed, mapping $\boldsymbol{\phi}$ only depends on the position of the physical nodes and therefore, so does Functional (1).

3.4. $\mathcal{L}_2$-disparity Measure

Given a curved high-order mesh and a manifold in the physical space, $\mathcal{M}^P$ and Σ, respectively, our objective is to quantify the disparity of the mesh and the parameterized manifold. We assume that the manifold Σ is parameterized by a continuously differentiable and invertible mapping (diffeomorphism)

$$\begin{aligned} \boldsymbol{\varphi} : \mathcal{U} \subset \mathbb{R}^m &\longrightarrow \Sigma \subset \mathbb{R}^n \\ \mathbf{u} &\longmapsto \mathbf{x} = \boldsymbol{\varphi}(\mathbf{u}), \end{aligned}$$

where $\mathcal{U}$ is the parametric space of the surface. In this work, we use the OpenCASCADE library [50] to retrieve the parameterization of the surfaces of a CAD model.

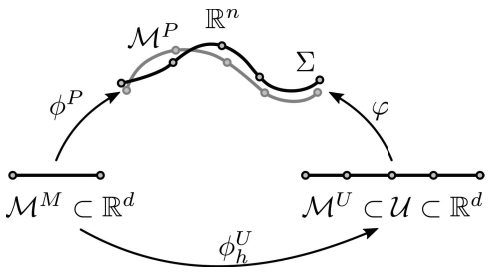

Fig. 2. $\mathcal{L}_2$-disparity measure between a mesh, gray line, and a manifold, black line. To compute the $\mathcal{L}_2$-disparity, an auxiliary parametric mesh, $\mathcal{M}^U$, is used.

We define the $\mathcal{L}_2$-disparity measure [45] of a physical mesh, $\mathcal{M}^P$, and a manifold, Σ, as

$$d\left(\mathcal{M}^p, \Sigma\right) = \inf_{\boldsymbol{\alpha}} \left\| \boldsymbol{\phi}^P - \boldsymbol{\varphi} \circ \boldsymbol{\alpha} \right\| = \inf_{\boldsymbol{\alpha}} \sqrt{\int_{\mathcal{M}^M} \left\| \boldsymbol{\phi}^P - \boldsymbol{\varphi} \circ \boldsymbol{\alpha} \right\|^2 \, \mathrm{d}\Omega}, \tag{2}$$

where $\|\cdot\|$ is the Euclidean norm, and $\boldsymbol{\alpha}$ are all the possible orientation-preserving diffeomorphisms between the master mesh, $\mathcal{M}^M$ and $\mathcal{U}$, see Figure 2. Note that the definition of the $\mathcal{L}_2$-disparity introduced in (2) is independent of the selected parameterization of Σ because we are taking the infimum over all the possible orientation-preserving diffeomorphisms between $\mathcal{M}^M$ and $\mathcal{U}$.

To compute the disparity between the mesh and the manifold, we define the functional

$$E_\Sigma(\boldsymbol{\phi}^P; \boldsymbol{\alpha}) = \left\| \boldsymbol{\phi}^P - \boldsymbol{\varphi} \circ \boldsymbol{\alpha} \right\|^2 \tag{3}$$

Note that

$$d\left(\mathcal{M}^P, \Sigma\right) = \sqrt{\inf_{\boldsymbol{\alpha}} E_\Sigma(\boldsymbol{\phi}^P; \boldsymbol{\alpha})}.$$

In order to minimize functional E_Σ, we take an element-wise polynomial approximation of the diffeomorphism $\boldsymbol{\alpha}$. That is, $\boldsymbol{\alpha}|_{\mathrm{e}^M} \approx \boldsymbol{\phi}^U|_{\mathrm{e}^M}$ such that

$$\begin{aligned} \boldsymbol{\phi}_h^U|_{\mathrm{e}^M} : \mathrm{e}^M &\longrightarrow \mathrm{e}^U \subset \mathcal{U} \\ \boldsymbol{\xi} &\longmapsto \mathbf{u} = \sum_{i=1}^{N_u} \mathbf{u}_i N_i^{\mathbf{u}}(\boldsymbol{\xi}), \end{aligned}$$

with $\mathcal{U}$ the parametric space of the manifold parameterization, and $\{N_i^{\mathbf{u}}\}_{i=1,\dots,n_u}$ a Lagrangian basis of polynomial shape functions of degree q. In fact, the mapping $\boldsymbol{\phi}_h^U$ characterizes a high-order mesh, $\mathcal{M}^U$, of polynomial degree q in the parametric space of the manifold, and the position of its nodes is $\mathbf{u}_i$, for $i = 1, \dots, N_U$. Note that the polynomial degree of the parametric mesh and the physical mesh can be different and, in general, are not the same. In an intuitive manner, the parametric mesh allows the alignment of the physical mesh with the parameterization of the geometric entity. Although we do not have yet a theoretical setting to select the value of q, it depends on the parameterization of the geometric entity, and the polynomial degree of the physical mesh, p. In our experience, if q is high enough the resulting meshes obtain optimal convergence rate. To this end, in all the presented examples we have set the polynomial degree of the parametric mesh as $q = p + 2$.

Since we approximate $\boldsymbol{\alpha}$ by $\boldsymbol{\phi}^U$, and $\boldsymbol{\phi}^U$ is determined by the position of the parametric mesh nodes, functional E_Σ in (3) also depends on the position of the parametric nodes. Thus, the minimization of functional E_Σ with respect to the parametric node coordinates leads to an approximation of the $\mathcal{L}_2$-disparity between the mesh and the manifold. Moreover, the minimization of functional E_Σ with respect to the physical node coordinates and the parametric node coordinates, leads to the mesh that *best* approximates the given manifold in terms of the proposed $\mathcal{L}_2$-disparity. Note that in this setup, the coordinates of the nodes are not restricted to be on the manifold Σ. That is, we do not seek a mesh that interpolates the manifold. We aim to obtain the non-interpolative high-order mesh that *best* approximates the given manifold in a weak sense.

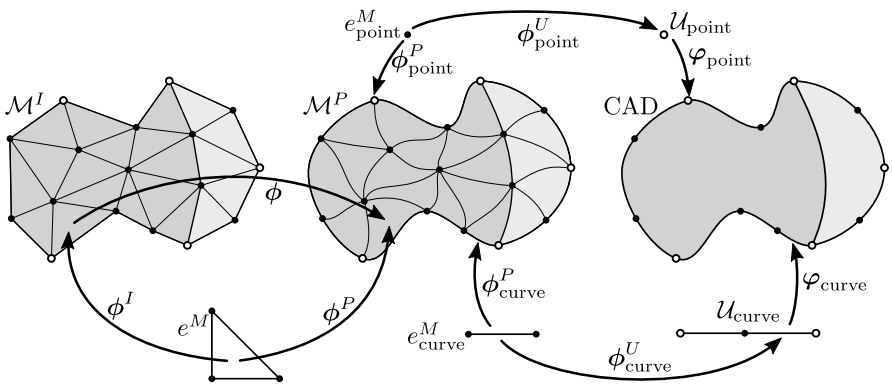

Fig. 3. Diagram of the involved mappings during the coupled optimization process of the mesh quality and the $\mathcal{L}_2$-disparity measure.

4. Quality and $\mathcal{L}_2$-disparity Coupled Optimization

In this section, we propose a framework to generate curved high-order meshes with optimal mesh quality and geometric accuracy. Figure 3 shows the diagram of the involved mappings during the coupled optimization process of the mesh quality and the $\mathcal{L}_2$-disparity measure. Our input data is a CAD model, Ω, composed of several geometric entities in such a way that

$$\Omega = \bigcup_{k=1}^{N} \Omega^k,$$

where each of the sub-entities are the different solids, surfaces, curves and points that compose the geometry. In addition, each sub-entity of the CAD model, Ω^k, is embedded in a manifold Σ_k parameterized by a continuously differentiable and invertible mapping (diffeomorphism)

$$\begin{aligned} \boldsymbol{\varphi}_k : \ \mathcal{U}_k \subset \mathbb{R}^{d_k} &\longrightarrow \Sigma_k \subset \mathbb{R}^3 \\ \mathbf{u} &\longmapsto \mathbf{x} = \boldsymbol{\varphi}_k(\mathbf{u}) \end{aligned},$$

where $\boldsymbol{\varphi}_k$ and d_k are the parameterization and the dimension of manifold Σ_k, and $\mathcal{U}_k$ is the corresponding parametric space.

We also consider a curved high-order mesh of polynomial degree p in the physical domain, $\mathcal{M}^P$, that approximates the CAD model, Ω, in such a manner that

$$\mathcal{M}^P = \bigcup_{k=1}^{N} \mathcal{M}^P_k,$$

where each $\mathcal{M}^P_k$ is a curved high-order mesh of polynomial degree p that approximates the corresponding geometric entity Ω^k. We consider that the physical mesh, $\mathcal{M}^P$, is defined in terms of a continuous element-wise polynomial diffeomorphism, $\boldsymbol{\phi}_P$ and that each of the sub-meshes $\mathcal{M}^P_k$ is defined as the corresponding restriction of $\boldsymbol{\phi}^P$

$$\boldsymbol{\phi}^P_k = \boldsymbol{\phi}^P|_{\mathcal{M}^M_k},$$

being $\mathcal{M}^M_k$ the mesh composed of all the master elements of the mesh $\mathcal{M}^P_k$. In order to compute the quality of the physical mesh $\mathcal{M}^P$, we have an ideal mesh, $\mathcal{M}^I$, that defines the optimal elements according to shape and size. Note that the physical mesh can also be defined as the deformation of the ideal mesh by the mapping $\boldsymbol{\phi}$, as seen in Section 3.3. Finally, in order to compute the disparity of the mesh $\mathcal{M}^P_k$ and the geometric entity Ω_k, we need a curved high-order mesh of polynomial degree q in the parametric domain of Ω^k, see Section 3.4.

The main objective of this work is to determine an optimal physical mesh, $\mathcal{M}^P$, in terms of mesh quality and geometric approximation. To this end, we define the functional

$$E_\mu(\boldsymbol{\phi}^P; \boldsymbol{\phi}^U_1, \dots, \boldsymbol{\phi}^U_N) = E_Q(\boldsymbol{\phi}) + \mu E_\Omega(\boldsymbol{\phi}^P_1, \dots, \boldsymbol{\phi}^P_N; \boldsymbol{\phi}^U_1, \dots, \boldsymbol{\phi}^U_N), \tag{4}$$

where $\boldsymbol{\phi} = \boldsymbol{\phi}^P \circ \left(\boldsymbol{\phi}^I\right)^{-1}$ and

$$E_\Omega(\boldsymbol{\phi}_1^P, \ldots, \boldsymbol{\phi}_N^P; \boldsymbol{\phi}_1^U, \ldots, \boldsymbol{\phi}_N^U) = \sum_{k=1}^{N} E_{\Omega_k}(\boldsymbol{\phi}_k^P, \boldsymbol{\phi}_k^U) \tag{5}$$

Taking into account Equations (2) and (5), we define the $\mathcal{L}_2$-disparity between a curved high-order mesh, $\mathcal{M}^P$, and a CAD model, Ω, as

$$d\left(\mathcal{M}^P, \Omega\right) = \sqrt{\inf_{\boldsymbol{\phi}_1^U, \ldots, \boldsymbol{\phi}_N^U} E_\Omega(\boldsymbol{\phi}_1^P, \ldots, \boldsymbol{\phi}_N^P; \boldsymbol{\phi}_1^U, \ldots, \boldsymbol{\phi}_N^U)} = \sqrt{\inf_{\boldsymbol{\phi}_1^U, \ldots, \boldsymbol{\phi}_N^U} \sum_{k=1}^{N} E_{\Omega_k}(\boldsymbol{\phi}_k^P, \boldsymbol{\phi}_k^U)} \tag{6}$$

Note that in Functional (4), the mapping $\boldsymbol{\phi}^P$ is determined in terms of the position of the physical mesh nodes. In addition, mappings $\boldsymbol{\phi}_k^U$ are determined by the position of the parametric nodes of the corresponding entity. Thus, Functional (4) is defined by the position of the physical mesh nodes, and by the position of the parametric nodes of all the geometric entities. For this reason, the optimization of Functional E_μ can be interpreted as finding the optimal position of the physical and parametric nodes that minimizes the mesh distortion and the $\mathcal{L}_2$-disparity measure. Note that in the present setup, we do not impose that the boundary physical nodes have to lie on their corresponding geometric entities. For this reason, after the optimization process ends, we obtain a non-interpolative mesh.

Parameter μ in Functional (4) weights the functional related with the quality and the functional related with the disparity. In our applications, instead of fixing a value for μ, we adopt a penalty strategy where μ is the penalty parameter. The penalty method, see [51], consists of solving a series of optimization problems with an increasing penalty parameter. To optimize each problem, we use Newton's method, with exact derivatives, to select an advancing direction, and a back-tracking line-search method, with the strong Wolfe condition, to compute the step length, see [51] for more details. After each optimization, we set the new penalty parameter as $\mu_{k+1} = \alpha\mu_k$. In our application, we are using $\alpha = 10$.

The proposed penalty method ends when a prescribed geometric precision, δ_{abs}, is achieved. If this geometric precision cannot be fulfilled, due to geometric and mesh quality constraints, we use an additional stopping criterion in which we check if the relative difference of the disparity functional in two consecutive optimizations is less than a given tolerance, δ_{rel}. That is, the two stopping criteria are

$$\left|E^*_{\Omega_i}\right| < \delta_{abs} \qquad \text{and} \qquad \frac{\left|E^*_{\Omega_{i-1}} - E^*_{\Omega_i}\right|}{\left|E^*_{\Omega_{i-1}}\right|} < \delta_{rel}.$$

In all the tested meshes, the algorithm has always terminated successfully using these stopping criteria, and we have obtained a geometrically accurate mesh composed of high-quality elements.

5. Examples

5.1. Optimal Convergence Rate

The objective of this example is to show that the proposed approach, the $\mathcal{L}_2$-disparity measure, Equation (6), converges to zero with optimal rate. Theoretically, the mesh should approximate the target geometry with a $\mathcal{L}_2$-disparity error proportional to h^{p+1}, being h a measure of the element size, and p the polynomial degree of the mesh. To this end, we generate a series of curved high-order meshes for the geometry shown in Figure 4.

Figure 5 presents a convergence rate analysis of the $\mathcal{L}_2$-disparity in an h-refinement process for polynomial degrees between one and four. At each h-step, there are twice as much elements approximating the inner circle as in the previous h-step. The left plot shows the convergence rate for the initial interpolative meshes. In the linear case, we obtain a sub-optimal convergence rate. However, in the $p = 2$ case, we get super convergence rate of the $\mathcal{L}_2$-disparity measure. For the case of $p = 3$, we obtain the same convergence rate as $p = 2$. Finally, for $p = 4$ the numerical errors inherent in the localization of the nodes on the curves of the CAD geometry prevent the correct convergence rate of the $\mathcal{L}_2$-disparity measure. The right plot in Figure 6 shows the convergence rate of the $\mathcal{L}_2$-disparity measure

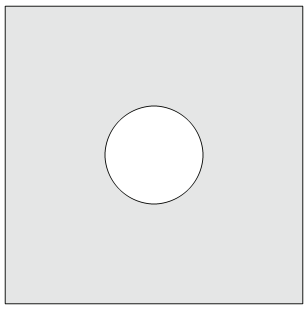

Fig. 4. CAD model of a square with a circular hole.

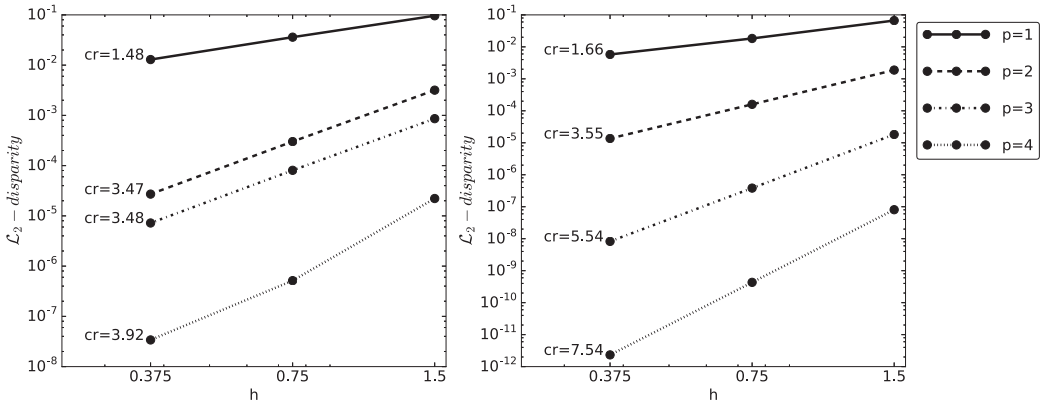

Fig. 5. Convergence rate of the $\mathcal{L}_2$-disparity for the original interpolative meshes (left) and the optimized non-interpolative ones (right).

Table 1. Minimum element quality of the initial and optimized meshes of the convergence rate analysis.

	$p=1$		$p=2$		$p=3$		$p=4$	
	initial	optimized	initial	optimized	initial	optimized	initial	optimized
$h=1.5$	0.994	0.989	0.910	0.972	0.890	0.973	0.889	0.974
$h=0.75$	0.993	0.993	0.976	0.992	0.975	0.984	0.975	0.994
$h=0.375$	0.991	0.994	0.990	0.998	0.990	0.998	0.989	0.998

for the optimized non-interpolative meshes. We point out that in all the cases except the linear one, we obtain super convergence of the proposed $\mathcal{L}_2$-disparity measure. That is, we are able to generate series of high-quality meshes that correctly approximate the target geometry in the sense of the $\mathcal{L}_2$-disparity measure. Note that we obtain a convergence rate proportional to $h^{2p-1/2}$. It is important to point out that the convergence rate of the disparity measure does not depend on the initial mesh. The initial mesh size and topology only determines the geometrical inaccuracy of the first approximation. In a convergence test, the rate is obtained from the slope in logarithmic scale between the disparity of the last two meshes.

Table 1 shows the minimum element quality for the initial interpolative meshes and the optimized non-interpolative meshes generated for the convergence rate analysis. Note that the only case where the minimum element quality decreases is the one corresponding to $h = 1.5$ and $p = 1$. For all the other cases, the minimum element quality has increased or is the same. This shows that we are able to generate a series of high-quality meshes that converge to the target geometry with the expected convergence rate.

Figure 6 shows the mesh generated for the case of $p = 4$ and $h = 0.375$. In Figure 6(a) we see the geometric error amplified by a factor of $5 \cdot 10^5$. Then, we optimize the mesh, see Figure 6(b), and the geometric error is reduced. To actually observe the magnitude of the geometric error, we amplify it by a factor of $5 \cdot 10^9$, see Figure 6(c).

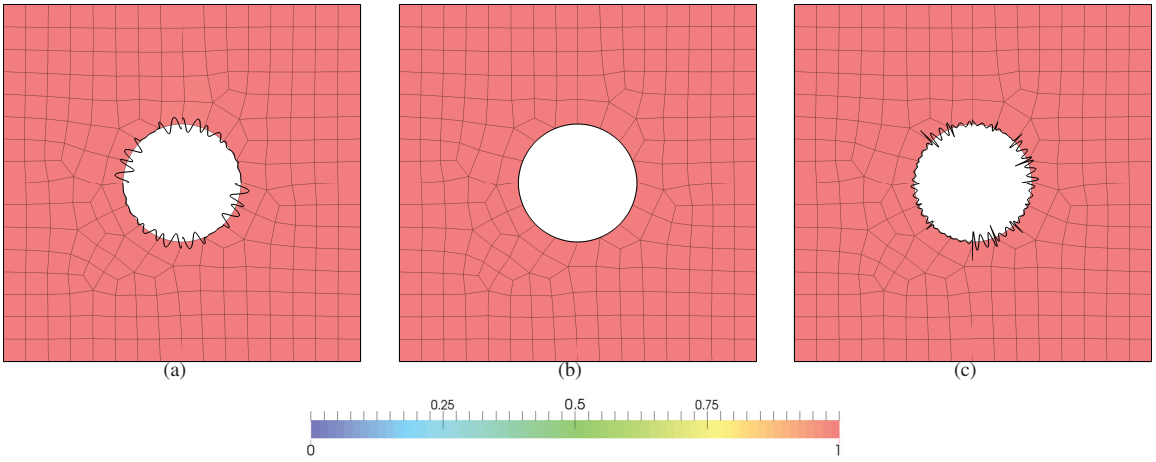

Fig. 6. Quadrilateral meshes of polynomial degree four, elements colored by quality, and geometric error at the boundary (thick line): (a) original interpolative mesh, geometric error amplified by a factor of $5 \cdot 10^5$; (b) optimized non-interpolative mesh, geometric error amplified by a factor of $5 \cdot 10^5$; and (c) optimized non-interpolative mesh, geometric error amplified by a factor of $5 \cdot 10^9$.

5.2. Sensitivity of the Method

The objective of this example is to show the sensitivity of the proposed penalty method when increasing the value of the penalty parameter. To this end, we have generated a triangular curved high-order mesh of polynomial degree seven around a NACA5507 airfoil profile. Figure 7(a) shows the initial mesh and the geometric error amplified by a factor of 100. The initial mesh contains one inverted element at the leading edge. In addition, the geometric error around the leading edge is the largest since the geometry is highly curved. When we apply the proposed optimization methodology, we obtain a high-quality non-interpolative mesh without any inverted elements, and the geometric error is decreased, see Figure 7(b).

Figure 8(a) shows the evolution of the $\mathcal{L}_2$-disparity measure against the minimum quality, along the different optimization problems of the proposed penalty method. Note that as we increase the penalty parameter, the minimum quality tends to decrease. On the one hand, the elements have to accommodate the curvature of the leading edge and, on the other hand, as the penalty parameter increases, the Hessian matrix of the functional in Equation 4 becomes ill-conditioned. However, it is worth to point out that the minimum quality in this mesh is around 0.7. Moreover, as the penalty parameter increase, the disparity measure decreases and therefore, the geometric accuracy increases.

5.3. Dealing with CAD models with gaps

In this example we show the curved high-order mesh generated on a brake disk, see Figure 8(b). The CAD model of this geometry is complex and there are gaps between the different edges and vertices of the model. That is, there are vertices that do not lie perfectly on the end points of its adjacent edges. We have to point out that this is a common situation in CAD models since the performed operations to create the model introduce numerical errors. In practical situations, the CAD model is considered valid if the gaps between adjacent entities are below a prescribed threshold. The objective of this example is to show that the proposed framework is able to handle real-case geometries that contain gaps. To this end, we generate a curved high-order triangular mesh of polynomial degree five for the brake disk. The initial mesh contain some inverted elements and large geometric errors around the high-curvature curves of the geometry, see Figure 9(a) for a detailed view of the mesh. When we apply the proposed optimization framework, we obtain a new mesh without any inverted elements and that better approximates the target geometry, see Figure 9(b). Note that the largest geometric errors are located around the vertices of the geometry. The reason is that these vertices do not perfectly lie at the end-points of their adjacent edges. That is, there is a gap around the vertices. Despite this difficulty, our proposed method is able to handle these cases and delivers a mesh without any inverted elements that better approximates the target domain than the initial interpolative mesh.

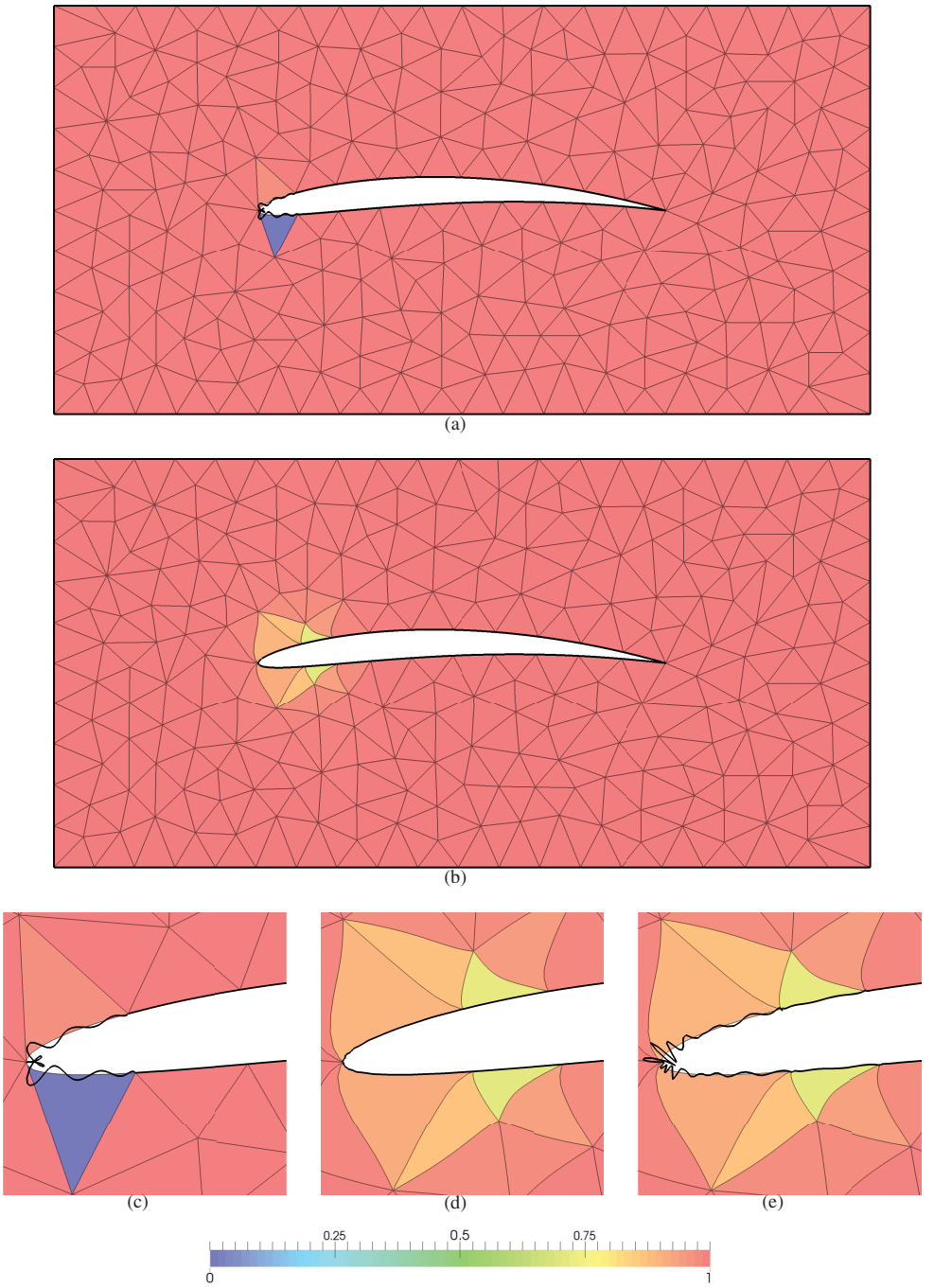

Fig. 7. Triangular meshes of polynomial degree seven, elements colored by quality, and geometric error at the boundary (thick line): (a) original interpolative mesh, geometric error amplified by a factor of 100; and (b) optimized non-interpolative mesh, geometric error amplified by a factor of 100. Detail of the leading edge for the (c) original interpolative mesh, geometric error amplified by a factor of 100; (d) optimized non-interpolative mesh, geometric error amplified by a factor of 100; and (e) optimized non-interpolative mesh, geometric error amplified by a factor of 2500.

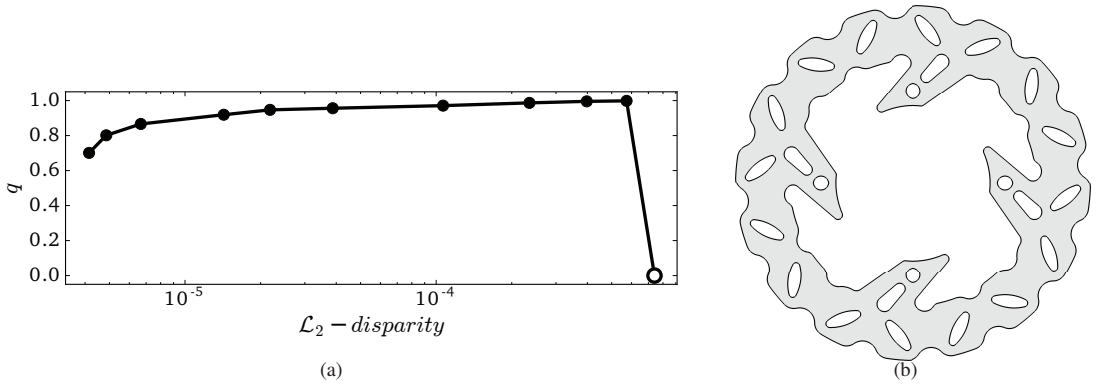

Fig. 8. (a) Evolution of the $\mathcal{L}_2$-disparity measure against the minimum quality of the mesh along the different optimization problems of the penalty method. The white dot points at the state of the initial mesh. (b) CAD model of a brake disk.

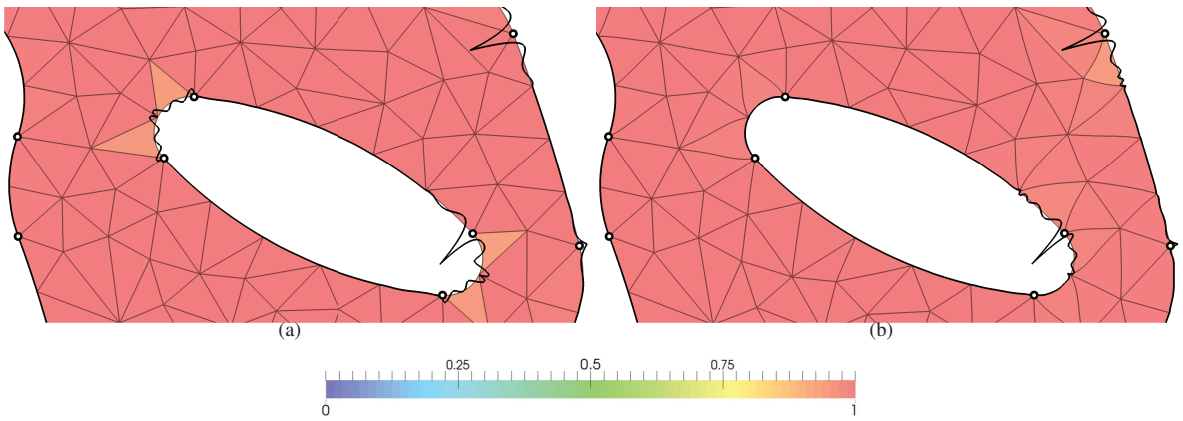

Fig. 9. Triangular meshes of polynomial degree four, elements colored by quality, and geometric error at the boundary (thick line): (a) original interpolative mesh, geometric error amplified by a factor of 10^4; and (b) optimized non-interpolative mesh, geometric error amplified by a factor of 10^4.

6. Conclusions

We have developed a new methodology to optimize a curved high-order mesh in terms of both element quality and geometric approximation. We have combined two objective functions, one that targets the element quality, and one that targets the proposed $\mathcal{L}_2$-disparity measure. Then, we optimize a non-linear objective function using the penalty method to generate an optimal mesh in the sense of high-quality elements and optimal geometric approximation. The optimized mesh does not have the boundary nodes on their corresponding geometric entities and therefore, the final mesh is non-interpolative. Note that non-interpolative meshes have the potential to be more accurate than interpolative ones.

To define the objective function related to the $\mathcal{L}_2$-disparity, we have additional degrees of freedom related to the parametric meshes. However, these additional degrees of freedom allow to define a method that is independent of the selected parameterization of the geometric entities. Moreover, as we have shown in the examples, the additional degrees of freedom allow to super-converge the distance of a curved high-order mesh to its target geometry. In addition, we have shown that the proposed approach can handle real-case geometries that contain gaps in their definition. In our work, the initial triangular and quadrilateral meshes are generated using Triangle [52] and gen4u [53], respectively. Note that any other available, linear or bilinear, mesh generator can be used.

The main drawback of the proposed optimization approach is that the penalty method can generate arbitrary ill-conditioned Hessian matrices when the penalty parameter increases. This may reduce the quality of the high-order mesh, since the relative weight of the function related to the quality is lower than the one related to the disparity as the penalty parameter increases. One possible solution is to apply an augmented Lagrangian technique to avoid and arbitrarily large penalty parameter while still obtaining an optimal geometric accuracy.

In general terms, the number of inner nodes is larger than the number of boundary nodes. Accordingly, the computational cost of the proposed non-interpolative technique is dominated by the cost of relocating the inner nodes. Therefore, we have observed that the computational cost is equivalent to other a posteriori mesh curving methods where usually, only the inner nodes are free to move.

In the near future, we will extend to three dimensions the proposed technique. The method can be extended since it relies on the minimization of two main ingredients: the disparity measure [45] and the mesh distortion [22,39]. Note that we have previously applied these two ingredients to three dimensional problems.

In this work, we have combined the minimization of the geometric disparity with the minimization of the regularized shape distortion measure. Note that other mesh curving methods could be combined with the same geometric disparity. The main difference would be the final location of the mesh inner nodes. Nevertheless, we consider that the convergence rate of the geometric accuracy would not be significantly changed since it would mainly be driven by the minimization of the disparity measure.

Acknowledgements

This research was partially supported by the Spanish Ministerio de Economía y Competitividad under grand contract CTM2014-55014-C3-3-R, and by the Government of Catalonia under grand contract 2014-SGR-1471. The work of the last author was supported by the European Commission through the Marie Sklodowska-Curie Actions (HiPerMeGaFlows project).

References

[1] B. Szabó and I. Babuška. *Finite Element Analysis*. John Wiley & Sons New York, 1991.
[2] C Schwab. *p-and hp-finite element methods: Theory and applications in solid and fluid mechanics*. Clarendon Press Oxford, 1998.
[3] MO Deville, PF Fischer, and EH Mund. *High-order methods for incompressible fluid flow*, volume 9. Cambridge University Press, 2002.
[4] JS Hesthaven and T Warburton. *Nodal Discontinuous Galerkin Methods: Algorithms, Analysis, and Applications*. Texts in Applied Mathematics. Springer, 2007.
[5] G Karniadakis and S Sherwin. *Spectral/hp element methods for computational fluid dynamics*. Oxford University Press, 2013.
[6] S. Sherwin and J. Peiró. Mesh generation in curvilinear domains using high-order elements. *Int. J. Numer. Meth. Eng.*, 53(1):207–223, 2002.
[7] P. E. Vos, S. Sherwin, and R. Kirby. From h to p efficiently: implementing finite and spectral/hp element methods to achieve optimal performance for low- and high-order discretisations. *J. Comput. Phys.*, 229(13):5161–5181, 2010.
[8] C. Cantwell, S. Sherwin, R. Kirby, and P. Kelly. From h to p efficiently: selecting the optimal spectral/hp discretisation in three dimensions. *Math. Model. Nat. Phenom.*, 6(3):84–96, 2011.
[9] R. Löhner. Error and work estimates for high-order elements. *Int. J. Numer. Meth. Fluids*, 67(12):2184–2188, 2011.
[10] M. Yano et al. *An optimization framework for adaptive higher-order discretizations of partial differential equations on anisotropic simplex meshes*. PhD thesis, Massachusetts Institute of Technology, 2012.
[11] R. Kirby, S. Sherwin, and B. Cockburn. To CG or to HDG: a comparative study. *J. Sci. Comput.*, 51(1):183–212, 2012.
[12] A. Huerta, X. Roca, A. Angeloski, and J. Peraire. Are high-order and hybridizable discontinuous Galerkin methods competitive? *Oberwolfach Rep.*, 9(1):485 – 487, 2012.
[13] R. Löhner. Improved error and work estimates for high-order elements. *Int. J. Numer. Meth. Fluids*, 72:1207–1218, 2013.
[14] Z.J. Wang, K. Fidkowski, R. Abgrall, F. Bassi, D. Caraeni, A. Cary, H. Deconinck, R. Hartmann, K. Hillewaert, H.T. Huynh, et al. High-order cfd methods: current status and perspective. *Int. J. Numer. Meth. Fluids*, 72(8):811–845, 2013.
[15] A. Huerta, A. Angeloski, X. Roca, and J. Peraire. Efficiency of high-order elements for continuous and discontinuous Galerkin methods. *Int. J. Numer. Meth. Eng.*, 96:529–560, 2013.
[16] F. Bassi and S. Rebay. High-order accurate discontinuous finite element solution of the 2D Euler equations. *J. Comput. Phys.*, 138(2):251–285, 1997.
[17] T. J. Barth. *Simplified numerical methods for gas dynamics systems on triangulated domains*. PhD thesis, Stanford University, 1998.
[18] S. Dey, M. Shephard, and J.E. Flaherty. Geometry representation issues associated with p-version finite element computations. *Comput. Meth. Appl. M.*, 150(1–4):39–55, 1997.
[19] X. Luo, M. S. Shephard, and J.-F. Remacle. The influence of geometric approximation on the accuracy of higher order methods. In *8th Int. Conf. Numerical Grid Generation in Computational Field Simulations*, 2002.

[20] D. Xue and L. Demkowicz. Control of geometry induced error in *hp* finite element (FE) simulations. I. Evaluation of FE error for curvilinear geometries. *Internat. J. Numer. Anal. Model.*, 2(3):283–300, 2005.
[21] R. Sevilla, S. Fernández-Méndez, and A. Huerta. NURBS–Enhanced Finite Element Method (NEFEM): a seamless bridge between CAD and FEM. *Arch. Comput. Methods Engrg.*, 18(4):441–484, 2011.
[22] A. Gargallo-Peir, X. Roca, J. Peraire, and J. Sarrate. Optimization of a regularized distortion measure to generate curved high-order unstructured tetrahedral meshes. *International Journal for Numerical Methods in Engineering*, 103(5):342–363, 2015.
[23] J. Shewchuk. What is a good linear finite element? interpolation, conditioning, anisotropy, and quality measures. *Preprint*, 2002.
[24] S. Dey, R. O'Bara, and M. S. Shephard. Curvilinear mesh generation in 3D. *Comput. Aided Design*, 33:199–209, 2001.
[25] X. Luo, M. S. Shephard, R. O'Bara, R. Nastasia, and M. Beall. Automatic p-version mesh generation for curved domains. *Eng. Comput.*, 20(3):273–285, 2004.
[26] X. Luo, M. S. Shephard, J.-F. Remacle, R. O'Bara, M. Beall, B. Szabó, and R. Actis. P-version mesh generation issues. In *Proc. 11th Int. Meshing Roundtable*, pages 343–354. Springer Berlin Heidelberg, 2002.
[27] M. S. Shephard, J. E. Flaherty, K. Jansen, X. Li, X. Luo, N. Chevaugeon, J.-F. Remacle, M. Beall, and R. O'Bara. Adaptive mesh generation for curved domains. *Appl. Numer. Math.*, 52(2-3):251–271, 2005.
[28] E.J. Nielsen and W.K. Anderson. Recent improvements in aerodynamic design optimization on unstructured meshes. *AIAA J.*, 40(6):1155–1163, 2002.
[29] T.A. Oliver. *A high-order, adaptive, discontinuous Galerkin finite element method for the Reynolds-Averaged Navier-Stokes equations*. PhD thesis, Massachusetts Institute of Technology, 2008.
[30] Z. Xie, R. Sevilla, O. Hassan, and K. Morgan. The generation of arbitrary order curved meshes for 3D finite element analysis. *Comput. Mech.*, 51:361–374, 2012.
[31] P.-O. Persson and J. Peraire. Curved mesh generation and mesh refinement using lagrangian solid mechanics. In *Proc. 47th AIAA*, 2009.
[32] P. L. George and H. Borouchaki. Construction of tetrahedral meshes of degree two. *Int. J. Numer. Meth. Eng.*, 90(9):1156–1182, 2012.
[33] X. Roca, A. Gargallo-Peiró, and J. Sarrate. Defining quality measures for high-order planar triangles and curved mesh generation. In *Proc. 20th Int. Meshing Roundtable*, pages 365–383. Springer International Publishing, 2012.
[34] A. Gargallo-Peiró, X. Roca, J. Peraire, and J. Sarrate. Defining quality measures for mesh optimization on parameterized CAD surfaces. In *Proc. 21st Int. Meshing Roundtable*, pages 85–102. Springer International Publishing, 2013.
[35] T. Toulorge, C. Geuzaine, J.-F. Remacle, and Jonathan Lambrechts. Robust untangling of curvilinear meshes. *J. Comput. Phys.*, 254:8 – 26, 2013.
[36] D. Moxey, M.D. Green, S.J. Sherwin, and J. Peiró. An isoparametric approach to high-order curvilinear boundary-layer meshing. *Computer Methods in Applied Mechanics and Engineering*, 283(0):636 – 650, 2015.
[37] D. Moxey, D. Ekelschot, Ü. Keskin, S.J. Sherwin, and J. Peiró. High-order curvilinear meshing using a thermo-elastic analogy. *Computer-Aided Design*, 72:130–139, 2016.
[38] M. Fortunato and P.E. Persson. High-order unstructured curved mesh generation using the winslow equations. *Journal of Computational Physics*, 307:1–14, 2016.
[39] E. Ruiz-Gironés, X. Roca, and J. Sarrate. High-order mesh curving by distortion minimization with boundary nodes free to slide on a 3D CAD representation. *Computer-Aided Design*, 72:52–64, 2016.
[40] J. M. Escobar, E. Rodríguez, R. Montenegro, G. Montero, and J. M. González-Yuste. Simultaneous untangling and smoothing of tetrahedral meshes. *Comput. Meth. Appl. Mech. Eng.*, 192(25):2775–2787, 2003.
[41] A. Gargallo-Peiró, X. Roca, and J. Sarrate. A surface mesh smoothing and untangling method independent of the CAD parameterization. *Comput. Mech.*, 53(4):587–609, 2014.
[42] S.P. Sastry, S.M. Shontz, and S.A. Vavasis. A log-barrier method for mesh quality improvement. In *Proc. 20th Int. Meshing Roundtable*, pages 329–346. Springer International Publishing, 2012.
[43] A. Gargallo-Peiró, X. Roca, J. Peraire, and J. Sarrate. A distortion measure to validate and generate curved high-order meshes on cad surfaces with independence of parameterization. *International Journal for Numerical Methods in Engineering*, 2015.
[44] A. Gargallo-Peiró, X. Roca, J. Peraire, and J. Sarrate. Distortion and quality measures for validating and generating high-order tetrahedral meshes. *Engineering with Computers*, 31(3):423–437, 2015.
[45] E. Ruiz-Gironés, J. Sarrate, and X. Roca. Defining an $\mathcal{L}_2$-disparity measure to check and improve the geometric accuracy of non-interpolating curved high-order meshes. *Procedia Engineering*, 124:122–134, 2015.
[46] J. Yin and C. Teodosiu. Constrained mesh optimization on boundary. *Eng Comput*, 24(3):231–240, 2008.
[47] A. Kelly, L. Kaczmarczyk, and C.J. Pearce. Mesh Improvement Methodology for 3D Volumes with Non-Planar Surfaces. In *Proc. 21st Int. Meshing Roundtable*, 2011.
[48] J.F. Remacle, J. Lambrechts, C. Geuzaine, and T. Toulorge. Optimizing the geometrical accuracy of 2D curvilinear meshes. *Procedia Engineering*, 82:228–239, 2014.
[49] T. Toulorge, J. Lambrechts, and J.F. Remacle. Optimizing the geometrical accuracy of curvilinear meshes. *Journal of Computational Physics*, 2016.
[50] Open CASCADE. Open CASCADE Technology, 3D modeling and numerical simulation. `www.opencascade.org`, 2012.
[51] J. Nocedal and S. Wright. *Numerical optimization*. Springer Verlag, 1999.
[52] Jonathan Richard Shewchuk. Delaunay refinement algorithms for triangular mesh generation. *Computational geometry*, 22(1):21–74, 2002.
[53] J. Sarrate and A. Huerta. Efficient unstructured quadrilateral mesh generation. *Int. J. Numer. Meth. Engrg.*, 49, 2000.